

# Correlation between X-ray Lightcurve Shape and Radio Arrival Time in the Vela Pulsar

A. Lommen<sup>1</sup>, J. Donovan<sup>1,2</sup>, C. Gwinn<sup>3</sup>, Z. Arzoumanian<sup>4,5</sup>, A. Harding<sup>4</sup>, M. Strickman<sup>6</sup>,  
R. Dodson<sup>7</sup>, P. McCulloch<sup>8</sup>, and D. Moffett<sup>9</sup>

## ABSTRACT

We report the results of simultaneous observations of the Vela pulsar in X-rays and radio from the RXTE satellite and the Mount Pleasant Radio Observatory in Tasmania. We sought correlations between the Vela’s X-ray emission and radio arrival times on a pulse by pulse basis. At a confidence level of 99.8% we have found significantly higher flux density in Vela’s main X-ray peak during radio pulses that arrived early. This excess flux shifts to the ‘trough’ following the 2nd X-ray peak during radio pulses that arrive later. Our results suggest that the mechanism producing the radio pulses is intimately connected to the mechanism producing X-rays. Current models using resonant absorption of radio emission in the outer magnetosphere as a cause of the X-ray emission are explored as a possible explanation for the correlation.

*Subject headings:* pulsars: X-ray – pulsars: radio – pulsars: individual(Vela)

## 1. Introduction

The Vela pulsar (PSR B0833–45) has been well-studied. Much observational work has been done to understand Vela’s emission in individual wavelength regions; e.g. the work

---

<sup>1</sup>Department of Physics and Astronomy, Franklin and Marshall College, Lancaster, Pennsylvania.

<sup>2</sup>Department of Astronomy, Columbia University, New York, New York.

<sup>3</sup>Department of Physics, University of California, Santa Barbara, California.

<sup>4</sup>NASA Goddard Space Flight Center, Greenbelt, Maryland.

<sup>5</sup>Universities Space Research Association, Columbia, Maryland.

<sup>6</sup>Code 7651.2, Naval Research Laboratory, Washington, DC.

<sup>7</sup>Observatorio Astronómico Nacional, Madrid, España

<sup>8</sup>University of Tasmania, Tasmania, Australia.

<sup>9</sup>Furman University, Greenville, South Carolina.

of Krishnamohan & Downs (1983, hereafter KD83) in the radio regime, observations by Oegelman, Finley, & Zimmerman (1993) in the X-ray regime, and studies by Kanbach et al. (1994) in the gamma ray regime. Observations of Vela’s spectrum allow for the possibility of both polar cap (Daugherty & Harding 1996) and outer-gap (Cheng, Ruderman, & Zhang 2000) models of emission. Vela’s pulse profiles in individual regions have been phase-aligned using the phase of the radio pulse across the optical, X-ray, and gamma ray wavelength bands (Harding et al. 2002, hereafter H02). This article works to further relate Vela’s high energy emission to its low-energy (radio) emission.

X-ray observations of Vela are challenging. Though Vela is the strongest gamma ray source in the sky, the pulsar’s spectral power drops off in the hard X-ray band, making its X-ray emission very difficult to detect. Additionally, the pulsed emission is overwhelmed by the bright but unpulsed background of the X-ray emission nebula in which the pulsar is embedded (Helfand, Gotthelf, & Halpern 2001).

The single-peaked pulse profile of the Vela pulsar in radio wavelengths is much simpler than its high energy counterparts, although several studies have revealed compound emission. KD83 detected peak-intensity dependent changes in the pulse-shape with the strongest pulses arriving earlier than the averaged profile. They conclude that the radio peak is composed of four different components originating at different heights in the emission cone with components lower in the magnetosphere arriving later. In this article one aspect we explore is whether a similar connection persists in the X-ray regime, i.e. whether the X-ray pulses associated with early-arriving radio pulses have a different shape and/or a different flux than others.

Related work on other pulsars includes experiments probing the relationship between the Crab pulsar’s “giant” pulsed emission and its gamma ray emission (Lundgren et al., 1995, hereafter Lu95) or its optical emission (Shearer et al., 2003, hereafter Sh03). They reached opposite conclusions. Lu95 observe no correlation within their sensitivity, indicating that variations in radio flux are caused by changes in radio coherence, which only affects the radio intensity. Sh03 observe a significant correlation, and they thus conclude that the increased emission in the optical and radio is caused by an increased pair production efficiency.

Patt et al. (1999) study pulse-to-pulse variability in the X-ray regime for the Crab pulsar, and they find the pulses to be steady to 7%. Using this result, as well as previous work showing that the Crab exhibits giant radio pulses roughly every two minutes, they conclude that the radio and X-ray emission mechanisms are not closely related, even though it is likely that the optical and X-ray emission regions exist in the same section of the magnetosphere (Patt et al. 1999).

Additional experiments linking pulsar emission in the radio and X-ray regimes have been performed by Cusumano et al. (2003) and Vivekanand (2001). Cusumano et al. show that in PSR B1937+21 there is close phase alignment between X-ray pulses and giant radio pulses, suggesting a correlation in their emission regions. Vivekanand, on the other hand, finds that the X-ray flux variations are so much smaller than those at radio wavelengths that they are inconsistent with the existence of any relationship between the charged emitters in the two wavelength regimes.

Giant radio pulses have not been shown to exist in Vela, but Johnston et al. (2001, hereafter J01) discovered microstructure and ‘giant micropulses’ in the Vela pulsar. The giant micropulses have flux densities no more than ten times the mean flux density and have a typical pulse width of  $\sim 400\mu s$ .

By doing a pulse-by-pulse analysis of the Vela pulsar in X-ray and radio wavelengths, we will show in this paper that the Vela pulsar’s X-ray and radio emission mechanisms must be related. We will discuss the X-ray and radio observations in §2, our analysis in §3, the effects of scintillation in §4, a discussion of interpretations in §5, and finally our conclusions and related future work in §6.

## 2. Observations

Our data consist of 74 hours of simultaneous radio and X-ray observations taken over three months at the Mount Pleasant Radio Observatory in Tasmania and with the RXTE satellite. The radio data were acquired during 12 separate observations between 30 April and 23 August, 1998.

The radio data were collected as part of the long term monitoring program of ten young pulsars, including Vela (Lewis et al. 2003). These data were collected with the 26m antenna at 990.025 MHz using the incoherently de-dispersed single pulse system (full description in Dodson, McCulloch, & Lewis, 2002). All individual pulses from Vela are detectable, and the pulse height, integrated area, and central time of arrival (for the solar-system barycenter) were calculated from cross-correlation with a high signal to noise template in the usual fashion.

The X-ray data were taken during the same three months, yielding 265 ks of usable simultaneous observation. For the purposes of this project, only top-layer data from RXTE’s Proportional Counter Units (PCUs) in Good Xenon mode in the energy range of 2-16 keV were used. Other filtering parameters included were standard RXTE criteria: elevation was greater than 10 degrees, offset was less than 0.02 degrees, the data were taken with at least

3 PCUs on, time since SAA was at least 30 minutes, and electron0 was less than 0.105.

### 3. Analysis

We filtered the X-ray photon arrival times and transformed them to the Solar System Barycenter (SSB) using the standard FTOOLS (Blackburn 1995) package. We calculated the pulsar phase at the time of each X-ray photon, using the radio pulsar-timing program TEMPO<sup>10</sup>, and the ephemeris downloadable from Princeton University<sup>10</sup>. We matched each X-ray photon with the radio pulse that arrived at the SSB at the same time. The precise time span associated with each radio pulse was given by our best model for arrival time of the peak of the radio pulse,  $\pm 0.5 \times$  the instantaneous pulse period calculated via the model. Photons arriving on the borderline were associated with the earlier pulse. We then compared pulse profiles for X-rays segregated according to the arrival time of the radio pulse.

Single radio pulses arrive at a range of times around the predicted arrival time, as KD83 found. The histogram of residual arrival times for radio pulses, relative to the prediction of our best model, is shown in Figure 1. In the figure, and in our analysis, the average residual from each 5-minute segment of data was subtracted from all the data in that segment in order to account for any systematic wandering of the pulse arrival times relative to our model. The distribution of arrival times is slightly skewed, with a tail at late arrival times, so that the mean of the distribution is slightly later than the mode (at the peak of the histogram), as Figure 1 shows. We divided all of the pulses into 10 deciles, by the residual phase of the radio pulse, with equal numbers of pulses in each decile. Figure 1 shows our division of the residual phase of the radio pulse into the deciles. The deciles are well mixed in time, i.e. no particular observing epoch dominates any decile. Removing the 5-minute average residual eliminates effects of long-term trends that might appear independently in the radio pulse-timing and X-ray photon counting data.

We formed an X-ray pulse profile, integrated from 2–16 keV, for each of the deciles of radio-pulse arrival times, from the X-ray photons associated with each. Figure 2 shows the 10 resulting X-ray profiles. Each profile contains 13 bins in phase with the radio peak being at the left edge of each plot on the border between bins 13 and 1. The X-ray profiles are significantly different; the X-ray pulse changes in shape with the arrival of the radio pulse. We denote the ten X-ray profiles by their “lateness”: profile 1 comprises the decile of X-ray photons from the earliest radio-pulse arrivals, and profile 10 the decile from the latest radio-pulse arrivals. In particular it appears that the first X-ray pulse is sharper and stronger in

---

<sup>10</sup>See <http://pulsar.princeton.edu/tempo>

the earlier deciles. Overall 2 distinct X-ray peaks are visible in each of the first 5 profiles, whereas in profiles 6-10 the two peaks are difficult to distinguish. In order to quantify these changes, we performed a number of statistical tests on these 10 profiles including a full Monte Carlo simulation described at the end of this section.

We observe no significant trend in total X-ray flux with lateness. Figure 3 shows total counts for each of the 10 deciles. From these data, we determine Pearson’s correlation coefficient of  $r = -.26$  of total X-ray counts with radio-pulse lateness with a confidence interval of 54%. Nominally, this is not distinguishable from the hypothesis of zero correlation. Note, however, that Pearson’s  $r$  is not necessarily the best statistic for this comparison, as we discuss below.

We do find that the total counts reported in Figure 3 are inconsistent with the Gaussian distribution expected for this limit of the Poisson distribution produced by shot noise, at 99.7% confidence, as determined from a  $\chi^2$  test. This suggests that there is indeed an evolution of X-ray profile with radio lateness. If we consider the counts in individual bins, we find that they do deviate from the mean more than one would expect from Poisson statistics, as well. A simple  $\chi^2$  test determines that in bins 2 and 3 we can reject the hypothesis of Poisson noise around the mean value with 81% and 83% confidence respectively. In other words, bins 2 and 3 show larger changes than we would expect a priori. The changes among the 10 profiles in each of the other 11 lateness bins are consistent with Poisson noise.

The  $\chi^2$  test, however, is not suited to detecting trends. In order to detect trends we look to Pearson’s correlation coefficient,  $r$  and its associated confidence interval. Pearson’s  $r$  has limited validity in our case because it usually assumes that both variables are drawn from random distributions with nearly Gaussian statistics. In our case, lateness is deterministic rather than random and Gaussian. Shot noise in the profile is random and Gaussian, but differences of the X-ray profile among deciles need not be. Nonetheless, this is a useful first step to take to estimate the significance of any trends. Note also that Pearson’s  $r$  itself, though widely used to measure the strength of a correlation, does not judge the existence of a correlation. We therefore place more stake in the confidence interval, although this involves additional assumptions about the variables correlated (Press et al. 1992). If our visual impression of the profiles is accurate we would expect that in the trough, made up of bins 12, 13 and 1, the correlations are positive (increasing counts with increasing lateness). All 3 bins do indeed show positive correlations, 0.29, 0.66 and 0.35 respectively with associated confidence intervals of 58%, 96% and 68%. In other words, 2 of the 3 bins show a significant (greater than  $1\sigma = 65\%$ ) correlation. Likewise we would expect that the first X-ray peak, made up of bins 2 and 3, would show negative correlations (decreasing counts with increasing lateness). Bins 2 and 3 do in fact show negative correlations of  $-0.73$  and  $-0.48$  with 98%

and 85% confidence, consistent with our interpretation of the first peak decreasing with lateness. The only other bin that displays a significant correlation is bin 8, which shows a negative correlation of  $-0.63$  with 95% confidence.

Next we looked to see if pairs of bins could be combined together to better detect the signal. Based on our results described above we were curious about whether the quantity  $Y_{i,a} = (c_{i2} + c_{i3}) - (c_{i12} + c_{i13})$  or  $Y_{i,b} = (c_{i2} + c_{i3}) - (c_{i13} + c_{i1})$  would show significant trends with lateness. Here  $c_{i1}, c_{i2}, c_{i3}, c_{i12}, c_{i13}$  are the measured counts in bins 1, 2, 3, 12, and 13, at lateness  $i$ .  $Y_{i,a}$  and  $Y_{i,b}$  effectively measure, for the 10 profiles, the height of the peak minus the trough and are shown in Figure 4. Via a simple  $\chi^2$  test we can reject with 97% confidence the hypothesis that the parent distribution of either of the  $Y$ 's is a constant at the mean value. More importantly Figure 4 shows a clear systematic trend of  $Y$  with lateness. A line fitted to the data and its associated Poisson uncertainty shown in Figure 4 yields a slope of  $m = -297$  and  $-308$  respectively with a formal 1-standard deviation uncertainty of  $\sigma = 76$  for both, so both represent (not independently)  $\sim 4$  standard deviation detections of a trend in these data. For the sake of completeness we tried all possible differences of pairs of adjacent bins. The next highest magnitude slope was 208, but this and all other significant correlations included some subset of bins 12, 13, 1, 2, and 3. The correlation coefficients and associated confidence intervals for  $Y_{i,a}$  and  $Y_{i,b}$  are  $-0.91$  at 99.97% and  $-0.84$  at 99.74%.

Given the limited validity of the Pearson's  $r$  coefficient with non-random, non-normally distributed data, we sought a more rigorous estimation of the possibility that such a significant trend would arise amongst 10 such profiles merely by chance, i.e. merely by random fluctuation of each bin around its mean. To answer this question we performed a Monte Carlo simulation with  $10^5$  realizations of the data. Each simulated data set consisted of 10 profiles, each of 13 bins. The counts in each bin were chosen as a Gaussian deviate of the X-ray pulse profile, averaged over lateness, and with variance set by Poisson statistics. Thus, in the simulated data sets all differences among the 10 profiles arose entirely from counting statistics. In each simulated data set, for every possible pair of summed adjacent bins ( $\{1,2 \ \& \ 3,4\}$ ,  $\{1,2 \ \& \ 4,5\}$  ...  $\{j,k \ \& \ n,o\}$ , with bins  $\{j,k\}$  adjacent and bins  $\{n,o\}$  adjacent: 66 pairs in all) we computed  $Y_i$ :

$$Y_i = c_{ij} + c_{ik} - (c_{in} + c_{io})$$

where  $i = 1$  corresponds to the earliest profile in terms of radio phase, and  $c_{ij}$  is the number of counts in the  $j$ th bin of the  $i$ th profile. For the set of points  $\{i, Y_i\}$  where  $m$  and  $\sigma$  are the slope and uncertainty of the best-fit straight line we computed the following statistic:

$$\Gamma = (m/\sigma)^2$$

As for the fit to our data described above, we weighted the data by the uncertainties as given by Poisson statistics. We then compared the largest  $\Gamma$  for each simulated data set to the

largest  $\Gamma$  for the actual data (16.4) and found a probability of 0.0024 that the correlation we observe could have been obtained by chance.

We tried other statistics to see if we could find one more sensitive to the presence of a correlation like that we observed. The most sensitive one included Pearson’s  $r$  as follows:

$$\Gamma' = r^2 + (m/\sigma')^2$$

where  $\sigma'$  is the  $\sqrt{\text{mean}(c_{ij} + c_{ik}, c_{il} + c_{im})}$ .  $\Gamma'$  yielded a significance of 0.0007.  $\Gamma'$  is more sensitive than  $\Gamma$  to the proximity of our data to the fitted line, so it yields a smaller probability of false detection. Regardless, we retain the more straightforward  $\Gamma$  as a conservative estimate of the significance of our result.

Of use in interpreting our results is knowledge of the character of the radio residuals by which we are binning the X-ray photons. KD83 did much work in this area, but one question they do not address directly is the following: if a particular pulse is “early”, what is the chance that the next pulse will also be early? We calculated the autocorrelation function of radio residual, shown in figure 5. The function is normalized by the autocorrelation at zero lag. The function at a lag of 1 pulse is represented by the left edge of the plotted curve, at a value of 0.066. The figure shows that the pulsar has very little “memory” of the lateness of the previous pulse, although it is interesting to note there is finite correlation out to 40 pulse periods.

#### 4. Scintillation

In contrast to effects intrinsic to the pulsar, scintillation is unlikely to produce the observed association, because it does not affect X-rays; scintillation might erase such a correlation but it cannot introduce it. Diffractive scintillation for Vela at our frequency has a characteristic bandwidth of 2 kHz (Gupta 1995), far smaller than our observing bandwidth of 6.4 MHz. We therefore average over  $\sim 3200$  independent scintillation elements. Refractive scintillation modulates flux density over a wide bandwidth and has timescale  $\sim 25$  days (Desai et al. 1992). This was shorter than the total span of the observations, but much longer than the span of any one observation. To combat any effect that this might have on the observed arrival times, we defined the 10 deciles separately for each observation; i.e. the specific values of residual that separated each of the 10 bins were calculated for each individual radio observation. Again, these cutoffs were defined in such a way that an equal number of radio pulses was associated with each decile.

We assumed that the pulsar was stationary relative to a refractive scintillation element during each single observation, and further tests to ensure that the length of the observation

was not a factor were performed by renormalizing the cutoffs using both one hour and five minute timespans. Reanalyzing the X-ray data in one hour segments did not significantly change our results, and the five minute spans were found to be too short to accurately represent Vela’s emission.

## 5. Discussion

The early radio emission could result from coherent radiation along a different set of field lines (i.e. more leading) or from radiation at a higher altitude, or both. The work of KD83 suggests both. The early radio emission may also result from stochastic fluctuations in the radio beam intensity which would lead to pulse arrival time changes by changing the shape of the radio beam as it takes a finite time to sweep across our line of sight.

Petrova (2003, and references therein) offers a physical model that could explain the observed relationship between the radio and X-ray emission. Her model suggests that resonant absorption of radio emission from the outer magnetosphere leads to an increase in the pitch angles and momenta of the secondary pairs, which then leads to optical and higher energy emission by spontaneous synchrotron radiation. How could this model produce a changing X-ray pulse shape? Due to the effects of rotation of the magnetosphere and aberration, the early radio emission can cross a larger number of higher altitude field lines and at larger angles, thereby maximizing the opportunity for absorption by particles on those field lines, and therefore the production of high-energy radiation. Conversely a late radio photon on a path almost directly along the magnetic pole may escape the magnetosphere with many fewer interactions, since it will cross fewer open field lines and at smaller angle. The details of the above are somewhat unimportant as our knowledge of the magnetosphere and the plasma therein is limited, but the point is that as different parts of the radio beam are active, resonant absorption may happen at different rates in different parts of the magnetosphere, causing continuous change in the shape of the observed X-ray emission.

More generally our results imply a connection between the radio and X-ray emission mechanisms for Vela that is not consistent with outer gap models. In these models, the high energy emission results from a gap connection to the pole opposite from that producing the radio emission. The pole and outer gap associated with the same set of field lines are not visible to one observer. It is not clear how a correlation could exist between the radio and high energy regimes in these models.

The giant micropulse emission observed by J01 would cause a single radio pulse to arrive about 1 ms early, so it is realistic to consider the possibility that the giant micropulse



emission is primarily responsible for the early arrival of the radio pulse. However, out of 20,085 pulses that J01 observed at 1413 MHz, 14 of them contained giant micropulses. So the giant micropulses may be influencing the first of our 10 deciles, but cannot contribute to the effect observed in the other 9 deciles. We conclude that Vela’s giant micropulse emission cannot be responsible for the effect presented here.

## 6. Conclusions and Future Work

We have evidence that links features of Vela’s X-ray emission with features of its radio emission. First, we find that X-ray pulses associated with early radio pulses show stronger emission at the main X-ray peak which is the sharper of the two. Similarly X-ray pulses associated with later radio pulses show stronger emission at the trough following the 2nd X-ray peak, a region in phase near the radio peak. The trend we measure has a 0.2% probability of appearing in the data by chance. We conclude that there is a close relationship between X-ray and radio emission in the Vela pulsar.

We plan to further characterize the relationship between the radio and high energy emissions of pulsars to identify their origins and constrain magnetospheric models. In particular, we will explore the dependence of radio-to-X-ray correlations on the radio frequency and polarization properties of individual Vela pulses, both of which carry information about emission altitudes. Similar observations of other pulsars also promise useful insights as probes of different magnetic field strengths and emission/viewing geometries.

Many thanks to Ben Stappers, Michael Kramer, Russell Edwards, Wim Hermsen, David Helfand, Paul Ray, Simone Migliari and Tiziana Di Salvo for helpful comments. AL is grateful for the hospitality of the Australia Telescope National Facility and for a Research Corporation Grant in support of this research. ZA was supported by NASA grant NRA-99-01-LTSA-070. CG acknowledges support of NSF-AST-9731584. AH acknowledges support from the NASA Astrophysics Theory Program. RD acknowledges support as a Marie-Curie fellow via EU FP6 grant MIF1-CT-2005-021873. This research has made use of data obtained from the High Energy Astrophysics Science Archive Research Center (HEASARC), provided by NASA’s Goddard Space Flight Center.

## REFERENCES

Blackburn, J. K. 1995, In ASP Conf. Ser. 77: Astronomical Data Analysis Software and

- Systems IV, R. A. Shaw, H. E. Payne, and J. J. E. Hayes, eds., p. 367
- Cheng, K. S., Ruderman, M., & Zhang, L. 2000, *ApJ*, 537, 964
- Cusumano, G., Hermsen, W., Kramer, M., Kuiper, L., Löhmer, O., Massaro, E., Mineo, T., Nicastro, L., & Stappers, B. W. 2003, *A&A*, 410, L9
- Daugherty, J. K., & Harding, A. K. 1996, *ApJ*, 458, 278
- Desai, K. M., Gwinn, C. R., Reynolds, J., King, E. A., Jauncey, D., Flanagan, C., Nicolson, G., Preston, R. A., & Jones, D. L. 1992, *ApJ*, 393, L75
- Dodson, R. G., McCulloch, P. M., & Lewis, D. R. 2002, *ApJ*, 564, L85
- Harding, A. K., Strickman, M. S., Gwinn, C., Dodson, R., Moffet, D., & McCulloch, P. 2002, *ApJ*, 576, 376
- Helfand, D. J., Gotthelf, E. V., & Halpern, J. P. 2001, *ApJ*, 556, 380
- Johnston, S., van Straten, W., Kramer, M., & Bailes, M. 2001, *ApJ*, 549, L101
- Kanbach, G., Arzoumanian, Z., Bertsch, D. L., Brazier, K. T. S., Chiang, J., Fichtel, C. E., Fierro, J. M., Hartman, R. C., Hunter, S. D., Kniffen, D. A., Lin, Y. C., Mattox, J. R., Mayer-Hasselwander, H. A., Michelson, P. F., von Montigny, C., Nel, H. I., Nice, D., Nolan, P. L., Pinkau, K., Rothenmel, H., Schneid, E., Sommer, M., Sreekumar, P., Taylor, J. H., & Thompson, D. J. 1994, *A&A*, 289, 855
- Krishnamohan, S., & Downs, G. S. 1983, *ApJ*, 265, 372
- Lewis, D. R., Dodson, R. G., Ramsdale, P. D., & McCulloch, P. M. 2003, In *ASP Conf. Ser.* 302: Radio Pulsars, M. Bailes, D. J. Nice, and S. E. Thorsett, eds., p. 121
- Lundgren, S. C., Cordes, J. M., Ulmer, M., Matz, S. M., Lomatch, S., Foster, R. S., & Hankins, T. 1995, *ApJ*, 453, 433
- Oegelman, H., Finley, J. P., & Zimmerman, H. U. 1993, *Nature*, 361, 136
- Patt, B. L., Ulmer, M. P., Zhang, W., Cordes, J. M., & Arzoumanian, Z. 1999, *ApJ*, 522, 440
- Petrova, S. A. 2003, *MNRAS*, 340, 1229
- Press, W. H., Teukolsky, S. A., Vetterling, W. T., & Flannery, B. P. 1992. *Numerical Recipes in C*, Cambridge University Press

Shearer, A., Stappers, B., O’Connor, P., Golden, A., Strom, R., Redfern, M., & Ryan, O.  
2003, *Science*, 301, 493

Vivekanand, M. 2001, *MNRAS*, 326, L33

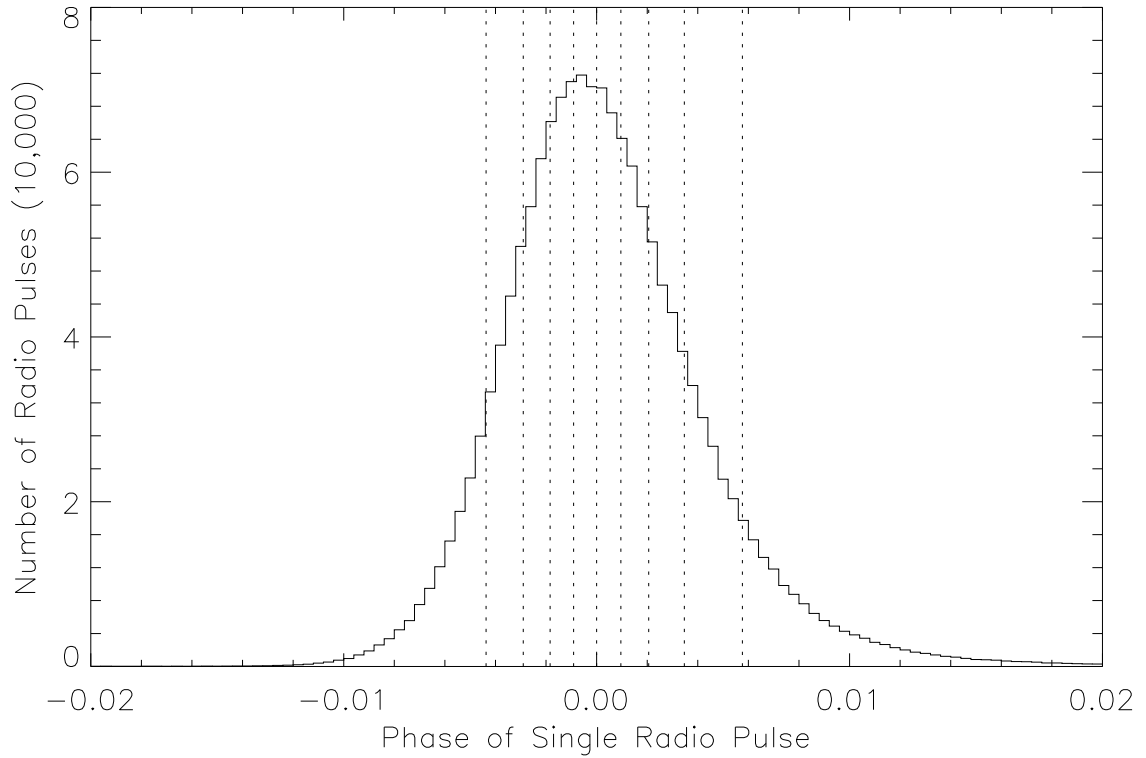


Fig. 1.— The number of radio pulses vs phase relative to a predictive long-term timing model over the entire data set. The dotted lines show the average position of boundaries of the 10 bins that were used to make the 10 profiles shown in Figure 2.

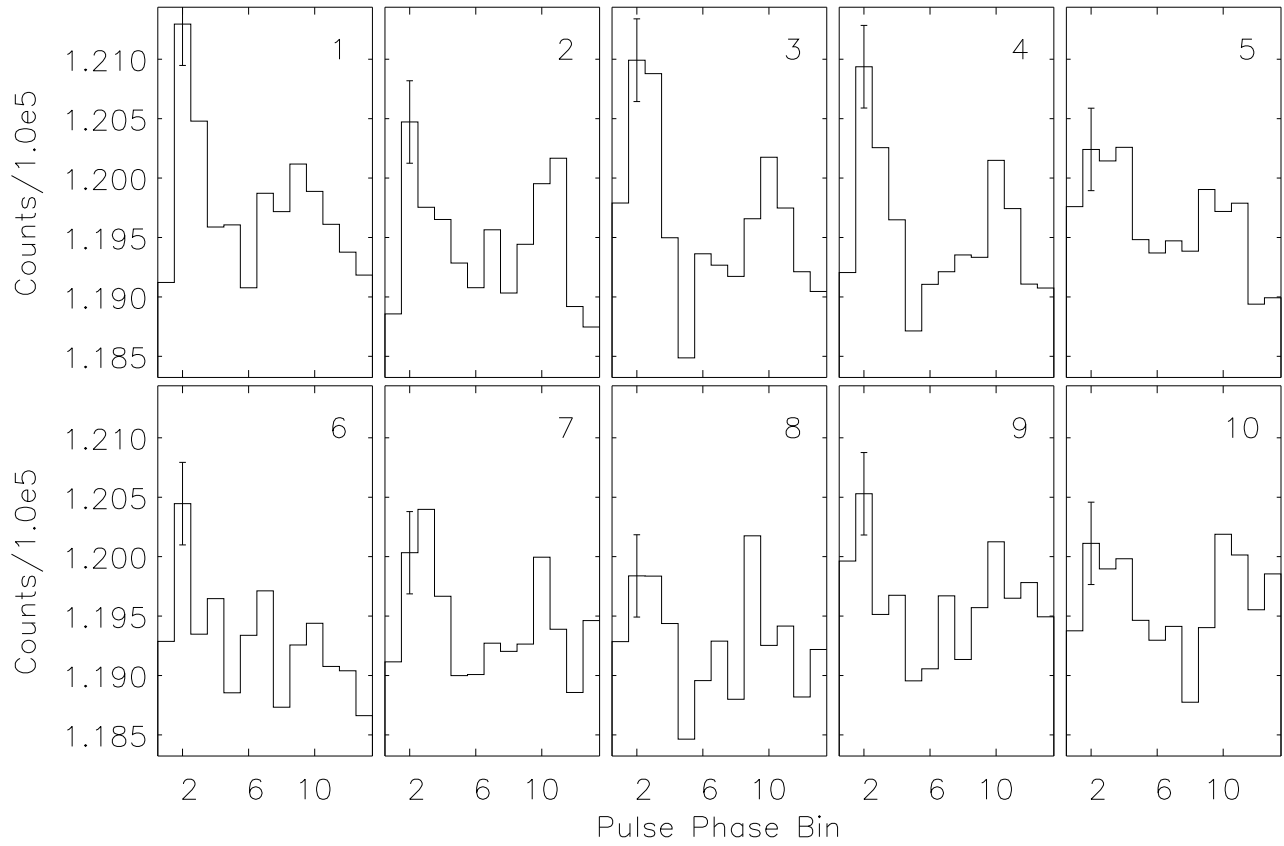


Fig. 2.— Full-period X-ray lightcurves for photons detected during radio pulse arrival times falling in the 10 decile bins shown in Figure 1.

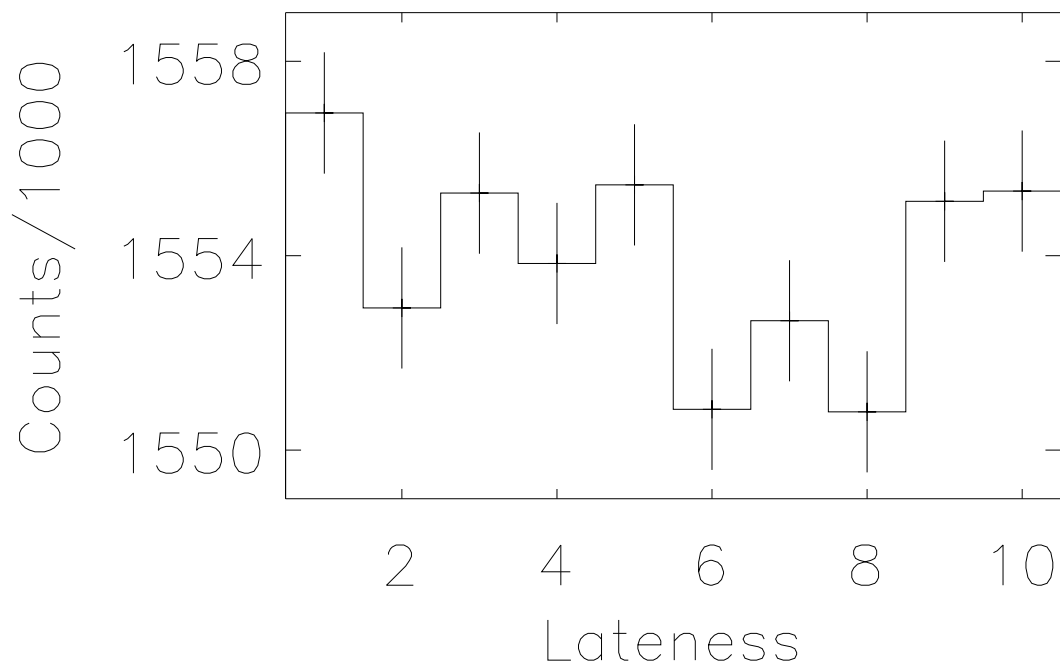


Fig. 3.— Total X-ray counts vs ‘lateness’ decile.

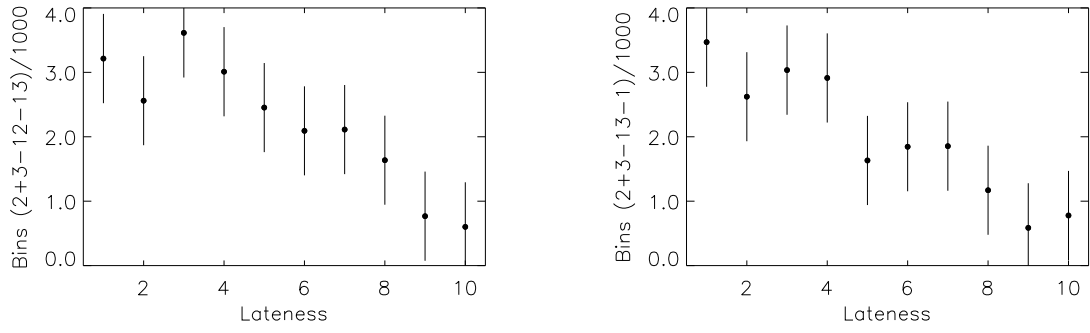


Fig. 4.— Left:  $Y_a = \text{bin2} + \text{bin3} - \text{bin12} - \text{bin13}$  vs the lateness of the radio pulse. Right:  $Y_b = \text{bin2} + \text{bin3} - \text{bin13} - \text{bin1}$  vs the lateness of the radio pulse.

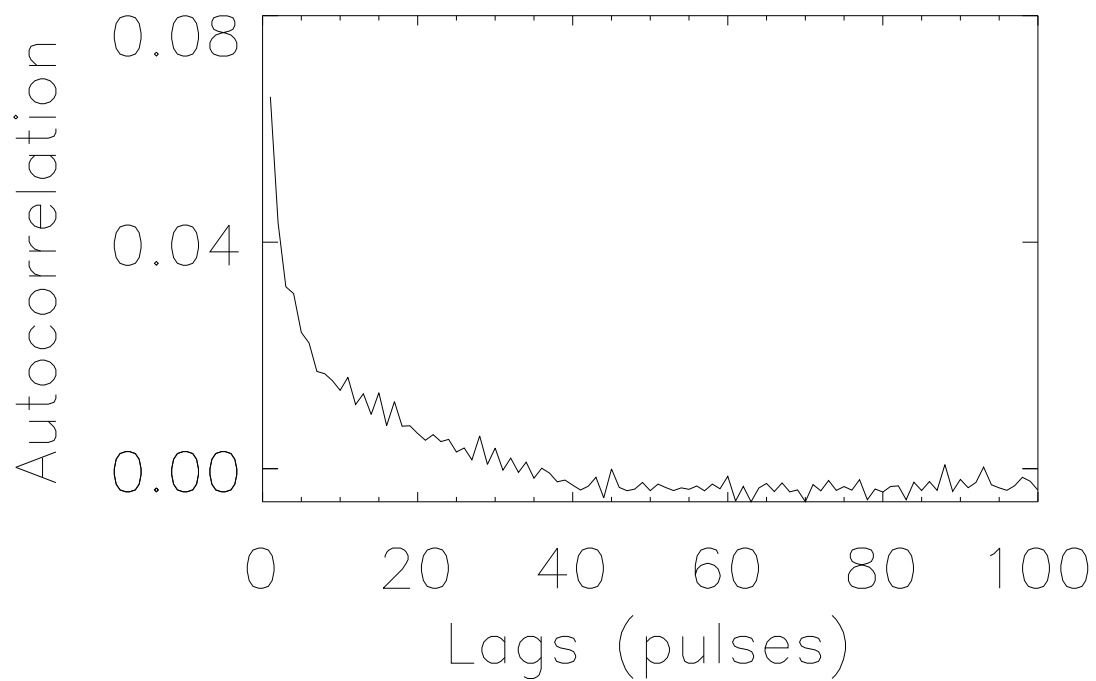


Fig. 5.— Autocorrelation of radio residual vs lags (pulses).